Available online at www.sciencedirect.com
ScienceDirect
Materials Letters 61 (2007) 1658–1661
materials letters
www.elsevier.com/locate/matlet

Structure and luminescence properties of TiO_2:Er^{3+} nanocrystals annealed at different temperatures

Jie Zhang [a,b], Xin Wang [a], Wei-Tao Zheng [a,*], Xiang-Gui Kong [b], Ya-Juan Sun [b], Xin Wang [b]

[a] *Department of Materials Science and Key Laboratory of Automobile Materials of MOE, Jilin University, Changchun, 130012, People's Republic of China*
[b] *Key Laboratory of Exited-State Process, Changchun Institute of Optics Fine Mechanics and Physics, Chinese Academy of Sciences, Changchun, 130033, People's Republic of China*

Received 10 March 2006; accepted 22 July 2006
Available online 10 August 2006

Abstract

Erbium doped TiO_2 nanocrystals with the structures of anatase, pyrochlore $Er_2Ti_2O_7$, and rutile, characterized by X-ray diffraction, have been obtained at different annealing temperatures from 300 °C to 900 °C. The nanocrystalline size for anatase TiO_2 is reduced with increasing doped erbium concentration. Following ultraviolet 325 nm irradiation, the intensity of the green emission is the most intense for the TiO_2:Er^{3+} nanocrystals with a structure of pyrochlore $Er_2Ti_2O_7$, which evolves from the structure of anatase annealed at 800 °C. Moreover, following ultraviolet 325 nm and infrared 980 nm irradiation, the visible emission spectra for the nanocrystals annealed at 900 °C change drastically. Correspondingly, the structure of anatase disappears, while that of rutile becomes dominant, which indicates that phase transformation occurs.

Keywords: TiO_2; Erbium ions; Luminescence; Nanocrystal

1. Introduction

Rare-earth-doped materials have been studied for more than three decades, which have potential applications for phosphors, display monitors, X-ray imaging, scintillators, lasers, and amplifiers for fiber-optic communications [1–3]. Recently, with the development of preparation technology of nanosize materials, nanomaterials, especially oxides, such as Y_2O_3, ZrO_2, and ZnO doped with rare-earth elements, have attracted much attention [4–6]. Doped titanium dioxide has also been the subject of numerous studies recently. For instance, due to its many useful optical, electrical, and photocatalytic properties, many investigations have concentrated on the effect of various dopants such as, Ce, Nb, Tb, Sn, Fe, Eu, and Mn on structural transformation of TiO_2 [7–13]. In very recent years, rare-earth-doped TiO_2 nanocrystallines with a low phonon energy ($<700\ cm^{-1}$) [14], which increases the number and the probability of radiative transitions for rare-earth-ion, have been focused. Furthermore, TiO_2 nanocrystals are non-toxic and might be candidates for the fluorescence label in biological applications due to their nanosizes. Also, it is of fundamental interest to better understand the luminescence properties of TiO_2 doped with various rare-earth materials. However, to the best of our knowledge, there are few reports on the relationships between the visible emission properties and the phase transformation of TiO_2 nanocrystals doped with rare-earth-ions although the infrared emission properties of doped TiO_2 have been studied, which might be applied in optical communication systems [15,16].

In this work, we investigate the anatase to rutile phase transformation of Er^{3+}-doped nanocrystal TiO_2 annealed at different temperatures (from 300 °C up to 900 °C), and the green and the red luminescence from intra-4*f* transition of erbium ions in TiO_2. We employ ultraviolet (UV) 325 nm and infrared (IR) 980 nm lasers to excite the nanocrystals annealed at different temperatures so that the visible downconversion and upconversion luminescence spectra can be obtained, respectively. In addition, in this letter, we attempt to explain the mechanism of structural change and luminescence properties for Er-doped TiO_2 nanocrystals.

2. Experimental

The TiO_2 nanocrystals doped with 1 mol%, 2 mol%, and 3 mol% erbium ions were prepared, respectively. Titanium

* Corresponding author. Tel./fax: +86 431 5168246.
E-mail address: WTZheng@jlu.edu.cn (W.-T. Zheng).

0167-577X/$ - see front matter © 2006 Elsevier B.V. All rights reserved.
doi:10.1016/j.matlet.2006.07.093

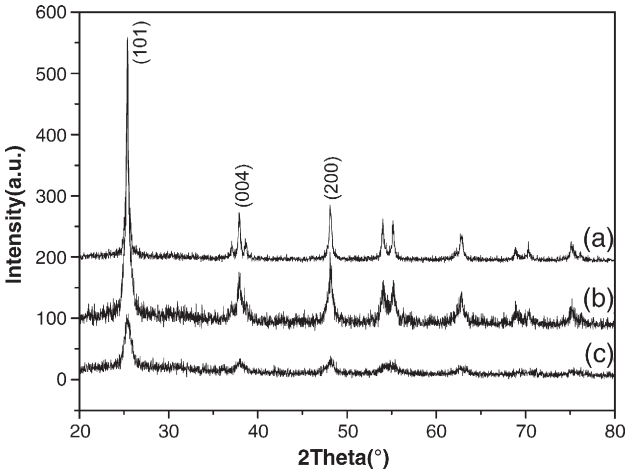

Fig. 1. X-ray diffraction patterns for (a) 1 mol%, (b) 2 mol%, (c) 3 mol% erbium doped TiO_2 nanocrystals.

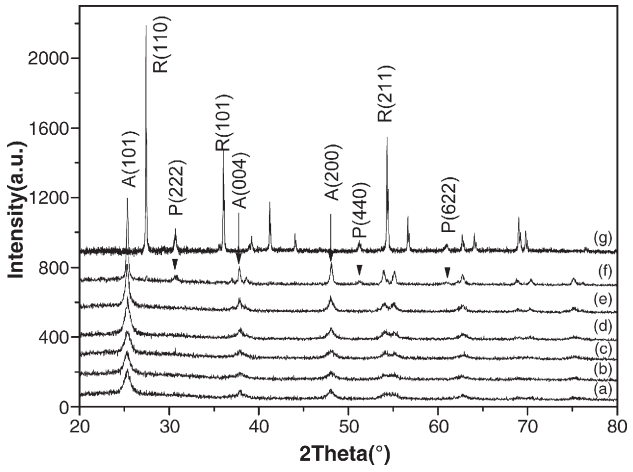

Fig. 3. X-ray diffraction patterns for 2 mol% erbium doped TiO_2 nanocrystals at various annealing temperatures (a) 300, (b) 400, (c) 500, (d) 600, (e) 700, (f) 800, and (g) 900 °C.

isopropoxide (Ti–$(OC_3H_7)_4$,AIfa) was hydrolyzed with vigorous stirring at room temperature according to an appropriate mole ratio of titanium to H_2O. After stirring for 1.5 h, the still damp sediment obtained from the resulting suspension filtered and washed three times with deionized water was put into deionized water to form slurry. Then appropriate tetramethylammonium hydroxide ($N(CH_3)_4OH$,AIfa) (TMNH) was added to the slurry. The system underwent vigorous stirring for 1 h at 85 °C after supersonic treatment for 5 min. Following that, an aqueous solution of $Er(NO_3)_3$ was added to the mixture drop by drop. After 30 min, hydrothermal processing was performed in 220 °C for 3 h. The resulting sediments were purified by centrifugation and washing with deionized water three times. Precursors were obtained after the purified sediments were dried in an oven at 80 °C. At last the nanosized samples were prepared in a muffle furnace for 1 h at different temperatures from 300 °C to 900 °C (step: 100 °C), respectively. All the samples were kept in air without any further precaution.

The structure of the samples was investigated by X-ray diffraction (XRD) (Bruker D8) using Cu Kα radiation. The surface morphology was observed by scanning electron microscopy (SEM) (JSM 6700F). Stokes and anti-Stokes emission spectra of Er^{3+} in the nanocrystals were measured using a Jobin–Yvon LabRam Infinity Raman spectrometer system equipped with 600 and 1800 grooves/mm holographic gratings, and a peltier air-cooled CCD detector. A 325 nm He–Cd laser and a 980 nm semiconductor solid laser were used as the excitation sources.

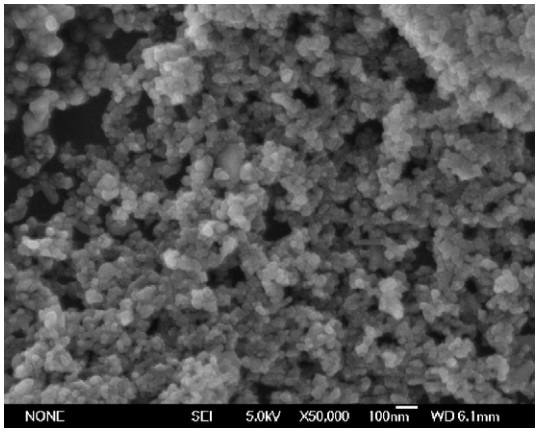

Fig. 2. Scanning electron micrograph of the TiO_2 nanocrystallines doped with 2 mol% Er^{3+} annealed at 700 °C.

3. Results and discussion

Fig. 1 shows the X-ray diffraction patterns for the three TiO_2 samples doped with 1 mol%, 2 mol%, 3 mol% erbium ions, respectively. The three strong peaks from (101), (004), (200) and the other peaks demonstrate that the samples have the body-centered tetragonal structure of the anatase phase, and Er_2O_3 crystalline phase does not appear. On the basis of the XRD patterns, full-width at half-maxima (FWHM) data could be analyzed by Scherrer formula [17] to determine the average particle sizes. It indicates that with increasing doped erbium ion concentration, the width of the peaks also increases. The average sizes of the TiO_2 nanocrystallines doped with 2 mol% Er^{3+} are below 40 nm, which is in agreement with those estimated by SEM, shown in Fig. 2. We can conclude that the increase in the concentration

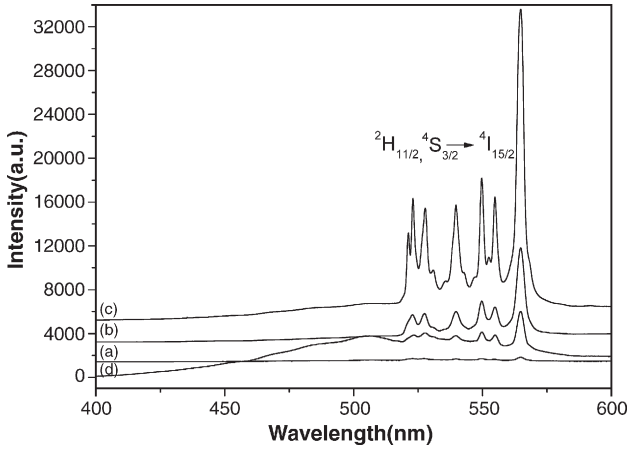

Fig. 4. Room-temperature Stokes emissions of Er^{3+} in the TiO_2 nanoparticles annealed at (a) 500, (b) 700, (c) 800, and (d) 900 °C under UV 325 nm excitation.

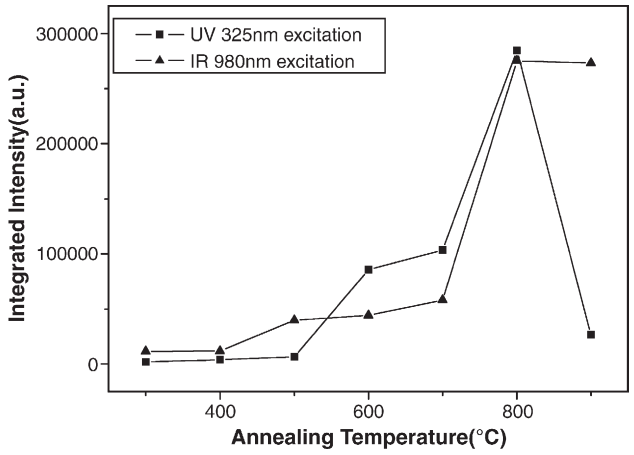

Fig. 5. Effect of annealing temperature on the green emissions from Er^{3+} in the TiO_2 nanoparticles under UV 325 nm and IR 980 nm excitation.

of doped erbium ions could decrease the size of TiO_2 nanocrystals, which is similar to TiO_2:Tb^{3+} [9].

Fig. 3 shows the X-ray diffraction patterns for 2 mol% erbium doped TiO_2 nanocrystals at various annealing temperatures (a) 300, (b) 400, (c) 500, (d) 600, (e) 700, (f) 800, and (g) 900 °C. For the samples annealed from 300 °C to 800 °C the intensities of peaks from TiO_2 with a structure of anatase increase. At annealing temperature of 800 °C, three additional weak peaks appear, which are contributed to the pyrochlore phase of $Er_2Ti_2O_7$ with a face-centered cubic structure. The anatase phase disappears at annealing temperature up to 900 °C. In contrast, the rutile phase with a tetragonal structure appears and becomes dominant, while the pyrochlore phase grows slightly. Considering that the atomic radius of Er (1.75 Å) is larger than that of Ti (1.45 Å) [18] and their valance is mismatched, erbium ions can hardly replace titanium ions in TiO_2 nanocrystals. Hence we believe that most of the erbium ions may be present on the interface/surface of TiO_2 nanocrystals. The pyrochlore phase of $Er_2Ti_2O_7$ is more easily formed on the interface/surface of TiO_2 nanocrystals than the rutile phase i.e. dopant erbium ions inhibited the nucleation and growth process of rutile within the anatase phase. It is well-known that the anatase to rutile phase transformation temperature for undoped TiO_2 is in the range of 700–900 °C [9,19]. However, various dopants,

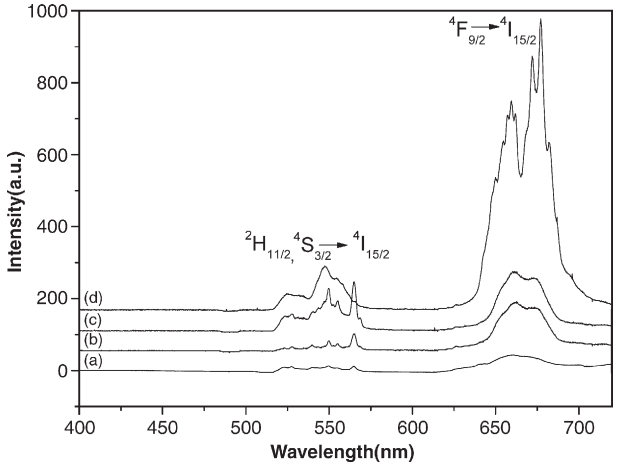

Fig. 6. Room-temperature anti-Stokes emissions of Er^{3+} in the TiO_2 nanoparticles annealed at (a) 500, (b) 700, (c) 800, and (d) 900 °C under IR 980 nm excitation.

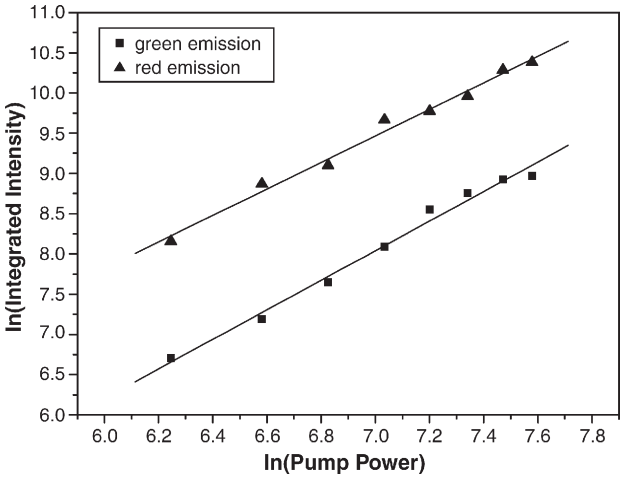

Fig. 7. Pump power dependence of the luminescence intensity of the upconversion green and red anti-Stokes emissions of Er^{3+} in the TiO_2 nanocrystals under 980 nm exitation.

including rare-earth-ions, have a great effect on the anatase to rutile phase transformation, either as accelerators or inhibitors [7–13]. Our results are nearly in agreement with that of Tb^{3+} doped TiO_2 reported by Zhang et al. [9]. The pyrochlore segregated phase on the interface/surface of TiO_2 nanocrystals may have a role in preventing the occurrence of transformation from the anatase phase into the rutile phase directly.

The well-known green band emission from erbium ions by UV 325 nm excitation, which is over the band gap of TiO_2 (3.2 eV) [18], shown in Fig. 4, belongs to $^2H_{11/2} \rightarrow {}^4I_{15/2}$, $^4S_{3/2} \rightarrow {}^4I_{15/2}$. The UV energy absorbed by TiO_2:Er^{3+} will transfer through the defect states of TiO_2 to erbium ions, resulting in visible emission. As annealing temperature increases from 300 °C to 800 °C, the intensity of the green emission increases, as shown in Fig. 5. From 300 °C to 500 °C, the intensity increases just slightly, which can be ascribed to some residual organics such as TMNH and hydroxyl groups that increase the probability of nonradiative relaxations of erbium ions. And some defects of the nanocrystals are also quenching centers. As the size of particles is within nanoscale, having a large proportion of surface area versus volume, the surface of the nanoparticles absorbs CO_2 and H_2O in air, whose vibrations could bridge the energy gap for quenching [20]. Thus, the multiphonon has an effect on luminescence quenching. As the temperature rises to 600 °C or 700 °C, most of the residual organics are decomposed and the defects decrease. As a result, the nanoparticles are better crystallized, and the influence of quenching is reduced. To our surprise, the intensity of the emission is the strongest at the annealing temperature of 800 °C. However, at 900 °C, the intensity of the luminescence decreases, rather than increases, accompanying an emission with a large wide peak. The strongest emission can be ascribed to the mixtures of the anatase and pyrochlore phase. The co-effects from the crystal field of the anatase and pyrochlore phase enhance the efficient emission of erbium ions. On the other hand, as the rutile phase appears, the anatase phase disappears. Correspondingly, as the phase transformation occurs for TiO_2, a large wide peak appears. This can be ascribed to the defect states, which decrease the luminescence of erbium ions since the lower efficiency of energy transfers from the defect states to erbium ions.

In order to reveal the relationship between the phase transformation and luminescence, the IR excitation source at 980 nm is employed and the upconversion luminescence is successfully obtained, as shown in Fig. 6. Comparing with UV excitation, IR excitation does not destroy

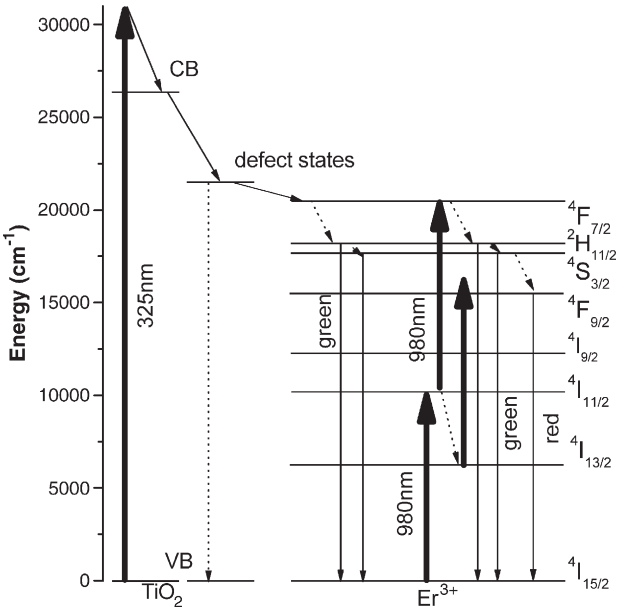

Fig. 8. Schematic diagram of the energy levels in the TiO_2 nanocrystals under 325 nm and 980 nm excitation.

the organism in which nanoparticles can be used as a label. The green band anti-Stokes emission is from $^2H_{11/2}\rightarrow{}^4I_{15/2}$, $^4S_{3/2}\rightarrow{}^4I_{15/2}$, while $^4F_{9/2}\rightarrow{}^4I_{15/2}$ provides the red band anti-Stokes emission. From 300 °C to 800 °C, the change of the intensity in the green and red emission is similar to that of the luminescence by UV 325 nm excitation (Fig. 5). However, the shape of the peak for the green and red emission at 900 °C changes significantly, which is more than expected. In green emission two large wide peaks are formed. In contrast, the sharp peaks in the red emission are observed, which are due to the split of crystal field for the rutile host, and the intensity at low wavelength, compared with the high one, decreases, although their intensities both increase. These discrepancies are ascribed to the different photoluminescence processes. To better understand the mechanism of the transition among $^2H_{11/2}$, $^4S_{3/2}$, and $^4F_{9/2}$ excited states, which are populated after IR irradiation, the upconversion luminescence intensity of the green ($^2H_{11/2}$, $^4S_{3/2}\rightarrow{}^4I_{15/2}$) and red ($^4F_{9/2}\rightarrow{}^4I_{15/2}$) emission has been measured as a function of the excitation power, as shown in Fig. 7. The upconversion output intensity (I_O) is proportional to the nth power of the infrared excitation intensity (I_{IR}): $I_O \propto I_{IR}^n$, where n is the number of IR photons absorbed per visible photon emitted [21,22]. The curve of $\ln(I_O)$ versus $\ln(I_{IR})$ yields a slope $n=1.83$ for ($^2H_{11/2}$, $^4S_{3/2}\rightarrow{}^4I_{15/2}$) transition, and $n=1.68$ for ($^4F_{9/2}\rightarrow{}^4I_{15/2}$) transition for all samples under investigation. High relaxation rate for multiphonon results in a slope lower than 2. Therefore, we believe that a two-photon process involved in the upconversion mechanism is responsible for the green and red emission.

For comparing the mechanism of green emission with that of red emission under UV and IR excitation, we display the schematic diagram of the energy levels for the erbium ion in the TiO_2 nanocrystals in Fig. 8. After UV 325 nm irradiation, the ions are excited into the conduction bands through the band gap of TiO_2, and subsequently decay to the defect states, followed by the energy transfer to the levels below the defect states such as the $^4F_{7/2}$ level, etc. The ions populating the $^4F_{7/2}$ level are not so stable that they will successively nonradiatively transit into the levels below. Nonradiation is achieved through the multiphonon decay process. From the level of $^2H_{11/2}$ and $^4S_{3/2}$, the green luminescence is emitted. Moreover, the emission from the defect states is observed, resulting in weakening the green emission since the energy transfer between the rutile TiO_2 and the erbium ions decreases. However, under IR 980 nm irradiation, the erbium ions in the ground state $^4I_{15/2}$ are excited to the $^4I_{11/2}$ level, and some excited ions absorb the photons to populate the $^4F_{7/2}$ level, i.e.: excited-state absorption (ESA). As the population of the $^4F_{7/2}$ level for erbium ions is not favored, rapid nonradiation will occur, leading to the decay for erbium ions into the level $^2H_{11/2}$, $^4S_{3/2}$, etc. below $^4F_{7/2}$. The green anti-Stokes emission comes from $^2H_{11/2}$, $^4S_{3/2}\rightarrow{}^4I_{15/2}$. The ions at level $^2H_{11/2}$ and $^4S_{3/2}$ nonradiatively decay into level $^4F_{9/2}$, which results in the red emission by the transition from $^4F_{9/2}$ to $^4I_{15/2}$. On the other hand, most of the excited ions at level $^4I_{11/2}$ nonradiatively decay into level $^4I_{13/2}$ for doped erbium ion TiO_2. Then the excited ions absorbed another photon populating the $^4F_{9/2}$ level. Consequently, a higher intensity for the red luminescence due to $^4F_{9/2}\rightarrow{}^4I_{15/2}$ transition, compared with that for the green luminescence, will be observed.

4. Conclusions

We have obtained the TiO_2:Er^{3+} nanocrystals with structures of anatase, a mixture of anatase and pyrochlore, and a mixture of rutile and pyrochlore at different annealing temperatures. Due to the strong effect of the crystal field, the optimum annealing temperature for the green emission is 800 °C, while it is 900 °C for the red upconversion through the two-photon absorption. Furthermore, the increase in doped erbium concentration reduces the size of TiO_2 nanoparticles.

References

[1] G. Blasse, B.C. Grabmaier, Luminescent Materials, Springer-Verlag, Berlin, 1994.
[2] R. Reisfeld, C.K. Jorgensen, in: R. Reisfeld, C.K. Jorgensen (Eds.), Laser and Excited State of Rare-Earths, Springer-Verlag, Berlin, 1977.
[3] M.J. Denjeka, B. Samson, Mater. Res. Soc. Bull. 8 (1999) 39.
[4] D. Matsuura, Appl. Phys. Lett. 81 (2002) 4526.
[5] E.D. Rosa-Cruz, L.A. Diaz-Torres, R.A. Rodriguez-Rojas, M.A. Meneses-Nava, O. Barbosa-Garcia, Appl. Phys. Lett. 83 (2003) 4903.
[6] X. Wang, X.G.. Kong, G. Shan, Y. Yu, Y. Sun, L. Feng, K. Chao, S. Lu, Y. Li, J. Phys. Chem., B 108 (2004) 18408.
[7] Q. Yan, X. Su, Y. Zhou, C. Ge, Rare Met. 24 (2005) 125.
[8] A. Burns, G. Hayes, W. Li, J. Hirvonen, J.D. Demaree, S.I. Shah, Mater. Sci. Eng., B 111 (2004) 150.
[9] H. Zhang, Y. Zhang, Y. Xu, Y. Wang, Acta Chimi. Sin. 61 (2003) 1813.
[10] S. Mahanty, S. Roy, S. Sen, J. Cryst. Growth 261 (2004) 77.
[11] S. Karvinen, Solid State Sci. 5 (2003) 811.
[12] Y. Chen, W. Cai, Y. Yu, D. Cui, X. Sun, J. Rare Earths 21 (2003) 26.
[13] R. Arroyo, G. Cordoba, J. Padilla, V.H. Lara, Mater. Lett. 54 (2002) 39.
[14] C. Urlacher, J. Mugnier, J. Raman Spectrosc. 27 (1996) 785.
[15] C.C. Ting, S.Y. Chen, J. Appl. Phys. 94 (2003) 2102.
[16] S. Jeon, P.V. Braun, Chem. Mater. 15 (2003) 1256.
[17] B.E. Warren, X-ray Diffraction, vol. 253, Dover, New York, 1990.
[18] M. Ishii, S. Komuro, T. Morikawa, J. Appl. Phys. 94 (2003) 3823.
[19] K. Kumar, K. Keizer, A. Burggraaf, J. Mater. Lett. 54 (1993) 1141.
[20] J.A. Capobianco, F. Vetrone, J.C. Boyer, A. Speghini, M. Bettinelli, J. Phys. Chem., B 106 (2002) 1181.
[21] M. Pollnau, D.R. Gamelin, S.R. Lüthi, H.U. Güdel, M.P. Hehlen, Phys. Rev., B 61 (2000) 3337.
[22] M.A. Chamarro, R. Cases, J. Lumin. 46 (1990) 59.